High-precision spot centroid positioning of high-frame-rate short-wave infrared images for satellite laser communication

FU Peng[1]，　HE Dao-Gang[2]，　LIU Jun[2]，　WANG Yue-Ming[1,2*]

（1. School of Physics and Optoelectronic Engineering，Hangzhou Institute for Advanced Study，
University of Chinese Academy of Sciences，Hangzhou 310024，China；
2. Key Laboratory of Space Active Opto-Electronics Technology，Shanghai Institute of Technical Physics，
Chinese Academy of Sciences，Shanghai 200083，China）

Abstract：The accuracy of spot centroid positioning has a significant impact on the tracking accuracy of the system and the stability of the laser link construction. In satellite laser communication systems, the use of short-wave infrared wavelengths as beacon light can reduce atmospheric absorption and signal attenuation. However, there are strong non-uniformity and blind pixels in the short-wave infrared image, which makes the image distorted and leads to the decrease of spot centroid positioning accuracy. Therefore, the high-precision localization of the spot centroid of the short-wave infrared images is of great research significance. A high-precision spot centroid positioning model for short-wave infrared is proposed to correct for non-uniformity and blind pixels in short-wave infrared images and quantify the localization errors caused by the two, further model-based localization error simulations are performed, and a novel spot centroid positioning payload for satellite laser communications has been designed using the latest 640×512 planar array InGaAs shortwave infrared detector. The experimental results show that the non-uniformity of the corrected image is reduced from 7% to 0. 6%, the blind pixels rejection rate reaches 100%, the frame rate can be up to 2000 Hz, and the spot centroid localization accuracy is as high as 0. 1 pixel point, which realizes high-precision spot centroid localization of high-frame-frequency short-wave infrared images.

Key words：satellite laser communication，spot centroid positioning，short-wave infrared，high frame rate，non-uniformity

面向卫星激光通信用高帧频短波红外图像高精度光斑质心定位

付　鹏[1]，何道刚[2]，刘　军[2]，王跃明[1,2*]
（1. 中国科学院大学 杭州高等研究院 物理与光电工程学院，浙江 杭州 310024；
2. 中国科学院上海技术物理研究所 空间主动光电技术重点实验室，上海 200083）

摘要：光斑质心定位的准确度对系统跟踪精度和激光链路搭建的稳定性有重要影响。在卫星激光通信系统中，采用短波红外波段作为信标光可以降低大气吸收，减少信号衰减。然而，短波红外图像中存在较强的非均匀性和盲元，这使得图像失真从而导致光斑质心定位精度下降。因此，短波红外图像光斑质心高精度定位具有重要的研究意义。本文提出了一种短波红外高精度光斑质心定位模型，对短波红外图像的非均匀性和盲元进行了校正，并量化了二者造成的定位误差；进一步基于模型进行了定位误差仿真，使用最新的 640×512 面阵 InGaAs 短波红外探测器，设计了用于卫星激光通信的新型光斑质心定位载荷。实验结果表明矫正后的图像非均匀性由 7% 降到 0.6%，盲元剔除率达到 100%，帧频可达 2 000 Hz，光斑质心定位精度高达 0.1 像素点，实现了高帧频短波红外图像的高精度光斑质心定位。

关　键　词：卫星激光通信；光斑质心定位；短波红外；高帧频；非均匀性

中图分类号：TN929.13　　　　　　　　　　　　　　　　文献标识码：A

FU Peng *et al*:High-precision spot centroid positioning of high-frame-rate short-wave infrared images for satellite laser communication

1 期

67

Introduction

With the advent of the information age, satellite communication, as an important part of the modern communication field, undertakes the important task of connecting the ground and space. However, conventional satellite microwave communications suffer from bandwidth bottlenecks in meeting high-speed communication requirements[1-2]. In contrast, satellite laser communication, as an emerging communication technology, uses high-frequency laser as a carrier with high satellite communication rate, no electromagnetic spectrum limitation, strong anti-jamming ability, good confidentiality and small volume and power consumption, etc. , which has become an effective means to alleviate the bottleneck of the microwave bandwidth of satellites and realize high-speed communication[3-5].

Foreign research on satellite laser communication field started earlier, Europe, the United States, Japan has carried out in-depth technical research[6-9]. Europe in 2008 through the "X-band terrestrial synthetic aperture radar" project test, realized the laser communication rate between satellites 5. 625 Gbit/s[10-11]. The "European Data Relay System", which started to provide services in 2016, is the first system in the world to realize the operational operation of inter-satellite laser communication technology[12-14]. The United States successfully implemented the "Lunar Laser Communication Demonstration and Verification" in 2013, which increased the transmission rate of the satellite underground link to 622 Mbit/s, and the transmission distance reached 400000 km[15-16]. Japan launched the Japan Relay Satellite System (JRSS) in 2020 to provide 1. 8 Gbit/s data relay service through inter-satellite laser link and Ka-band feeder link[17-20]. Domestic research on satellite laser communication started late, but in recent years has made a series of important progress. In 2011, China realized the first star-ground laser communication test, through the "Ocean II" satellite carrying the laser communication terminal developed by Harbin Institute of Technology, to realize the communication distance of 2000 km and 504 Mbit/s communication rate, filling the gaps in the domestic star-ground laser communication test. Subsequently, a number of satellites, such as Mozi, Tiangong-2, Practice 13, Practice 20, etc. , have also carried laser communication terminals for technical verification[21].

The satellite laser communication system consists of three basic subsystems: the optical system, the following aiming system and the communication system. Due to the small divergence angle of satellite laser communication, it is necessary to rely on optical systems and high-precision following systems to establish the link[22-24]. Among them, the tracking system is the core of laser communication, including coarse tracking unit, fine tracking unit and advance unit, which is used to realize the aiming, capturing and tracking of the optical signals of space beacons. In the tracking system, high-precision spot centroid localization is crucial for the aiming, capture and tracking process.

Currently, commonly used algorithms for spot centroid localization include grayscale weighting, ellipsoid fitting, and Gaussian surface fitting[25]. The grayscale weighting method considers the relationship between pixel values and weights, but requires high symmetry of the spot; the ellipse fitting method treats the spot as an ellipse and fits the centroid using the least-squares method, but it may lead to a large error in the case of asymmetric spot intensity; and the Gaussian surface fitting method simulates the point diffusion function of the imaging process through the Gaussian function, which provides a better stability. Researchers Rakesh Singh, Joni *et al.* localized the center of the spot by means of Gaussian surface fitting and achieved sub-pixel level accuracy, which is superior to the conventional center centroid localization method[26]. However, these algorithms are mainly based on general image designs with poor centroid localization accuracy and are only adapted to bands with good image non-uniformity.

The use of short-wave infrared bands as beacon light reduces atmospheric absorption and signal attenuation compared to general images, making it suitable for use in fine tracking units. However, there are strong non-uniformity and blind pixels in the short-wave infrared image, which cause serious interference to the centroid positioning of the spot. Yang *et al.* combined the laser footprint image and detector observation data to reduce the non-uniformity interference and thus improve the spot localization accuracy, but the localization will be affected by the accuracy of the laser footprint, and the resistance to the satellite jitter and atmospheric interference is weak[27]. Bao *et al.* proposed a pixel response flat field model and correction method for CMOS image sensors based on point scale area to reduce the non-uniformity of infrared images, but the method ignores the effect of blind pixels, and the model is more complex and unfavorable to hardware implementation and poor real-time performance[28].

In order to tackle the challenge of high-precision spot centroid localization for short-wave infrared beacon light in satellite laser communication, we introduce a model for high-precision spot centroid localization in short-wave infrared. This model aims to investigate the impact of short-wave infrared image non-uniformity and blind pixels on spot centroid localization. Additionally, we design a high-frame-frequency payload for short-wave infrared spot centroid localization in satellite laser communication by utilizing a newly developed high-sensitivity 640×512 faceted array InGaAs short-wave infrared detector. With this solution, we are able to achieve high-precision spot centroid localization in short-wave infrared images. The load also supports image correction and centroid positioning under the detector open window, which is adapted to the needs of satellite laser communication, and the positioning accuracy reaches 0. 1 pixel point, which can be widely used in actual engineering practice. The research of this paper can better promote the development of the field of satellite laser communication, improve the performance and stability of the satellite communication system, and provide effective technical

means and theoretical guidance for the realization of high-speed and reliable satellite communication.

1 Short-wave infrared spot centroid positioning model

1. 1 Infrared imaging positioning principle

The information flow of the satellite laser communication spot imaging and localization system can be represented by Fig. 1. First，the energy of the short-wave infrared beacon light is transmitted through the atmosphere and reaches the optical system. In the optical system，the infrared light is modulated to form a solid image plane on the focal plane. The focal plane detector then captures the infrared image on the real image plane and transmits it to the information acquisition circuitry of the back-end electronics system. The information acquisition circuit receives the analog signal output from the detector using a signal with high input impedance，performs the necessary conditioning and filtering processes on this signal，and quantizes it with high precision. Finally，the quantized digital infrared image raw data is transferred to the FPGA for further processing to find out the spot centroid position.
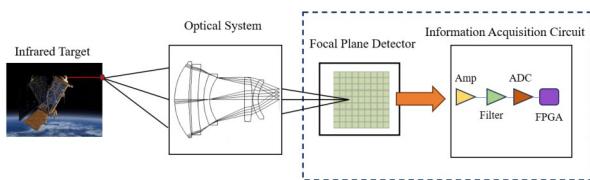

Fig. 1   Short-wave infrared imaging system
图1   红外成像系统

Ideally，when the focal plane detector is subjected to uniform illumination radiation，the response of each pixel is exactly the same. However，due to the inconsistency of semiconductor materials，mask errors，defects and process factors，there are inconsistent response differences between different detection units in the infrared focal plane array. These factors lead to the non-uniformity of the photoelectric conversion characteristic curve and dark noise，and blind pixels will appear in severe cases[29-31]，as shown in Fig. 2. At the same time，temperature variations can also affect the array elements. These factors can lead to the phenomenon of non-uniformity in the detector signal，which affects the centroid positioning accuracy.

1. 2 Degradation model

In the short-wave infrared imaging system，the spot centroid localization is mainly disturbed by non-uniformity noise and blind pixel noise. we expect to recover the ideal infrared image as much as possible to eliminate the interference of non-uniformity noise and blind pixel noise，and improve the centroid localization accuracy. Therefore，we model the two main interference noises，and the infrared image degradation model is expressed as
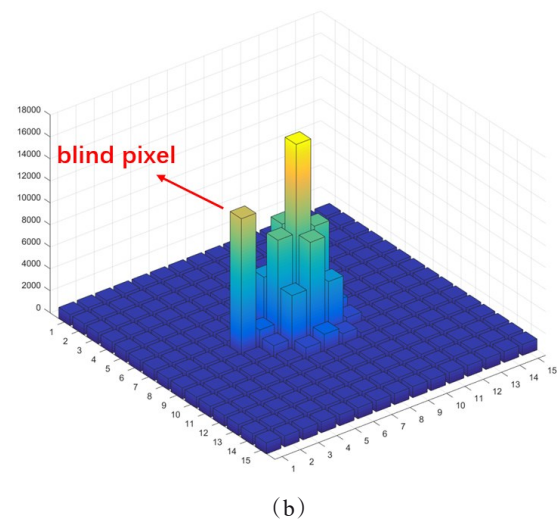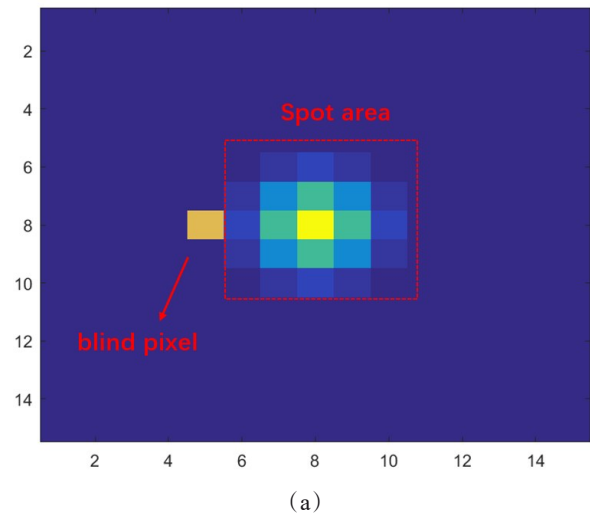
$$Z = S + B + \delta \qquad , \quad (1)$$

Fig. 2   Schematic diagram of a blind pixel with a Gaussian spot：(a)two-dimensional diagram；(b)three-dimensional diagram
图2   盲元与高斯光斑示意图：(a)二维示意图；(b)三维示意图

where Z denotes a short-wave infrared image disturbed by noise，S denotes an ideal image without noise，B denotes non-uniformity noise，and δ denotes random blind meta-noise.

1. 3 Correction method

Non-uniformity noise B can be categorized into relatively stable time-dimension non-uniformity noise and more random non-uniformity noise. The response of an infrared detector is linear to some extent，including the response gain and bias nonuniformity. Therefore，in this paper，the two-point correction method is used to correct the nonuniformity，and a response straight line is fitted based on the response values of the detector image pixels acquired at two different irradiance levels to correct the nonuniformity at other temperature points. The image S_1 after correction for non-uniformity can be expressed as：

$$S_1(i,j) = K(i,j)Z(i,j) + Q(i,j) \qquad , \quad (2)$$

where $K(i,j)$ is the gain correction coefficient，$Q(i,j)$ is

the offset correction coefficient, and i,j represents the pixel point position, both of which can be calculated by Eqs. (3) and (4), respectively:

$$K(i,j) = \frac{\overline{Z^{\varphi2}} - \overline{Z^{\varphi1}}}{Z_{(i,j)}^{\varphi2} - Z_{(i,j)}^{\varphi1}} \quad , \quad (3)$$

$$Q(i,j) = \overline{Z^{\varphi1}} - K(i,j)Z_{(i,j)}^{\varphi1} \quad , \quad (4)$$

where $Z^{\varphi2}$ is the mean value of all pixel points of the detector response averaged image at high energy level, $\overline{Z^{\varphi1}}$ is the mean value of all pixel points of the detector response averaged image at low energy level. $Z_{(i,j)}^{\varphi2}$ is the response value of the detector response averaged image at point (i, j) at high energy level, and $Z_{(i,j)}^{\varphi1}$ is the response value of the detector response averaged image at point (i, j) at low energy level.

For the blind pixel noise, this paper adopts the method of weighting neighboring pixels by using the mean value of their 4-neighborhood non-blind pixel points to replace the value of the blind pixel point, thus further eliminating the blind pixel noise on top of eliminating the non-uniformity noise.

1. 4　Spot centroid positioning

The calculation of the spot centroid mainly consists of two steps: coarse positioning and fine positioning. Coarse positioning refers to obtaining the location of the maximum value of the spot pixels, while fine positioning mainly uses the nine pixels in the center of the spot to obtain the sub-pixel coordinates of the centroid using the Gaussian surface fitting method. For short-wave infrared images, the spot centroid positioning is calculated as shown in Eq. (5):

$$f(x,y) = A \exp\left(-\frac{(x - x_0)^2 + (y - x_0)^2}{B}\right) \quad , \quad (5)$$

where $f(x, y)$ is the pixel point gray value and (x_0, y_0) is the centroid corresponding to the ideal spot image. Taking the logarithm on both sides of Eq. (5), we can get:

$$\ln f(x,y) = \ln A - \frac{(x - x_0)^2 + (y - y_0)^2}{B} \quad , \quad (6)$$

The centroid center point and its four-pixel points in horizontal and vertical directions are taken for fitting as shown in Fig. 3.
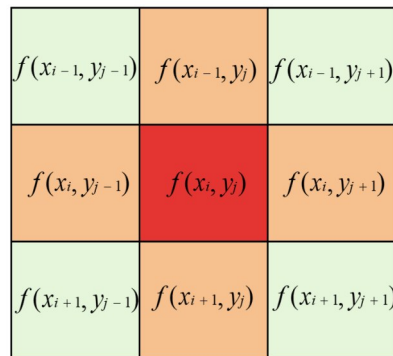

Fig. 3　Pixel point of spot centroid
图3　质心像素点

In the x-direction there are

$$\begin{cases} \ln f(x_i - 1,y_j) = \ln A - \dfrac{(x_i - 1 - x_0)^2 + (y_j - y_0)^2}{B} \\ \ln f(x_i,y_j) = \ln A - \dfrac{(x_i - x_0)^2 + (y_j - y_0)^2}{B} \\ \ln f(x_i + 1,y_j) = \ln A - \dfrac{(x_i + 1 - x_0)^2 + (y_j - y_0)^2}{B} \end{cases} \quad .(7)$$

Gaussian fitting calculates the coordinates at sub-pixel level, so (x_i, y_i) can be set as the coordinate origin, and Eq. (7) can be simplified as:

$$\begin{cases} \ln f(x_i - 1,y_j) = \ln A - \dfrac{(1 + x_0)^2 + (y_j - y_0)^2}{B} \\ \ln f(x_i,y_j) = \ln A - \dfrac{x_0^2 + (y_j - y_0)^2}{B} \\ \ln f(x_i + 1,y_j) = \ln A - \dfrac{(1 - x_0)^2 + (y_j - y_0)^2}{B} \end{cases} \quad . \quad (8)$$

Solving the above equation gives

$$x_0 = \frac{[\ln f(x_i + 1,y_j) - \ln f(x_i - 1,y_j)]/2}{[\ln f(x_i,y_j) - \ln f(x_i - 1,y_j)] + [\ln f(x_i,y_j) - \ln f(x_i + 1,y_j)]} \quad . \quad (9)$$

The same reasoning leads to

$$y_0 = \frac{[\ln f(x_i,y_j + 1) - \ln f(x_i,y_j - 1)]/2}{[\ln f(x_i,y_j) - \ln f(x_i,y_j - 1)] + [\ln f(x_i,y_j) - \ln f(x_i,y_j + 1)]} \quad . \quad (10)$$

Thus, the sub-pixel coordinates of the spot centroid are calculated, and combined with the coarse positioning coordinates, the final spot centroid coordinates are obtained.

1. 5　Centroid positioning error

Conventional spot centroid localization algorithm do not consider non-uniformity and blind pixels effects, and the spot obeys a Gaussian distribution, which can be directly used for centroid localization using Eq. (6). While in the short-wave infrared spot centroid localization, the infrared image usually has non-uniformity as well as blind pixels noise, which causes errors in the spot centroid coordinates derived from Eq. (6). To further quantify this error, the centroid localization of the infrared image after non-uniformity and blind pixels correc-

tion is first expressed as follows according to Eqs. (1)(2)(5):

$$K(x,y)Z(x,y) + Q(x,y) - \delta(x,y) ==$$
$$A \exp\left(-\frac{(x - x_0')^2 + (y - y_0')^2}{B}\right) \quad , \quad (11)$$

where x_0' and y_0' represent the centroid coordinates of the spot. Due to the influence of non-uniformity and blind noise, the coordinates of the centroid positioning will be deviated. The deviation in the x direction and y direction of the centroid is expressed as:

$$\begin{cases} \Delta x = |x_0' - x_0| \\ \Delta y = |y_0' - y_0| \end{cases} \quad . \quad (12)$$

Define operator $\Gamma(x_i, y_j) = \ln(K(x_i, y_j)z(x_i, y_j) + Q(x_i, y_j) - \delta(x_i, y_j))$. According to Eqs. (11), (12),

the centroid positioning error caused by non-uniformity and blind pixels in the x and y directions can be obtained as follows：

$$\Delta x = \left| \frac{[\Gamma(x_{i+1},y_j) - \Gamma(x_{i-1},y_j)]/2}{2\Gamma(x_i,y_j) - \Gamma(x_{i-1},y_j) - \Gamma(x_{i+1},y_j)} - \frac{[\mathrm{In}f(x_{i+1},y_j) - \mathrm{In}f(x_{i-1},y_j)]/2}{2\mathrm{In}f(x_i,y_j) - \mathrm{In}f(x_{i-1},y_j) - \mathrm{In}f(x_{i+1},y_j)} \right| \quad , \quad (13)$$

Similarly，in the y direction，there is

$$\Delta y = \left| \frac{[\Gamma(x_i,y_{j+1}) - \Gamma(x_i,y_{j-1})]/2}{2\Gamma(x_i,y_j) - \Gamma(x_i,y_{j-1}) - \Gamma(x_i,y_{j+1})} - \frac{[\mathrm{In}f(x_i,y_{j+1}) - \mathrm{In}f(x_i,y_{j-1})]/2}{2\mathrm{In}f(x_i,y_j) - \mathrm{In}f(x_i,y_{j-1}) - \mathrm{In}f(x_i,y_{j+1})} \right| \quad . \quad (14)$$

2 Experimental results and analysis

2.1 Experimental setup

InGaAs short-wave infrared（SWIR）detectors have wide spectral coverage，low noise and spectral response in typical SWIR bands[32-35]. This paper focuses on the experimental validation using the newly developed short-wave 640×512 faceted InGaAs detector R&D load from Shanghai Institute of Technology and Physics，Chinese Academy of Sciences，which has an image center distance of 15 μm，a spectral response range of 0.95-1.7 μm，a peak sensitivity of ≥0.8 A/W，and a detection rate of ≥5×10^{12} cm•Hz/W. It consists of a low-noise readout circuit，an InGaAs photosensitive chip with a P-I-N structure，and a first-stage thermoelectric cooler，which is packaged in a metal form，as shown in Fig. 4.

The block diagram of the FPGA software system used for the load design is shown in Fig. 5，which contains the detector driver and image data acquisition module，serial communication module，temperature control module，Flash read/write control module，DDR read/write control module，image correction module，image transmission module and centroid extraction module. The system provides timing drive for the detector，and then uses AD to collect the analog signal output by the detector to convert it into a digital signal. Based on the model，Flash and DDR are used to correct the non-uni-
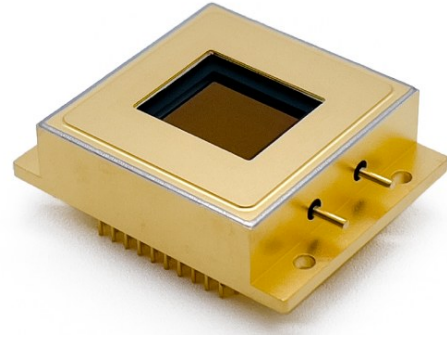

Fig. 4 The schematic diagram of shortwave 640 × 512 planar array InGaAs detector
图4 短波640×512面阵InGaAs探测器示意图

formity and blind pixels of the image with the help of correction data. The corrected image is subjected to threshold segmentation and spot target detection. After the spot target is detected，the centroid is obtained by using the Gaussian surface fitting method in the positioning model and transmitted to the satellite master.

2.2 Non-uniformity and blind pixel correction results

Figure 6 shows the original image output by the detector and the corrected image. It can be seen that the original image has obvious non-uniformity and more blind pixels，and after correction，the non-uniformity of the image is significantly improved and blind pixels disappear.

Figure 7 shows the distribution of blind pixels before and after image correction. It can be seen that a large number of blind pixels are distributed in the image before correction. After correction，the blind pixels in the central area of the image disappear，and only a few blind pixels are distributed on the edge of the image. This is due to the fact that the points on the edge of the detector are easily disturbed by the stray light reflection of the detector frame in the process of obtaining different energy level images to generate correction data.

When the infrared uniform radiation input，the non-uniformity of the infrared imaging system of the M-row N-column detector can be expressed as：
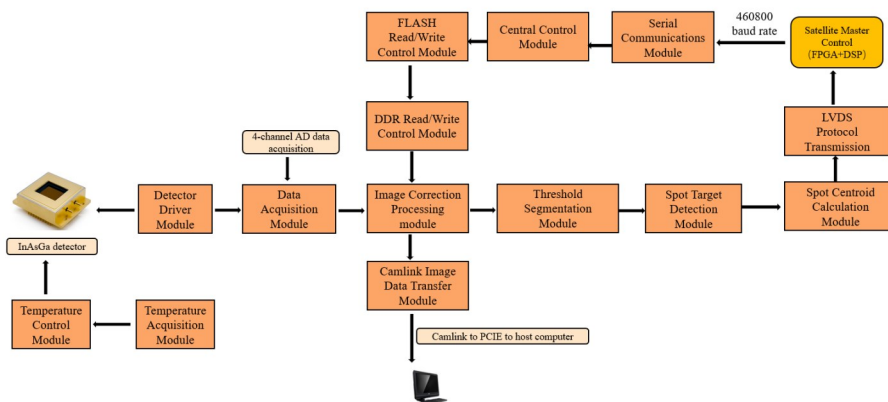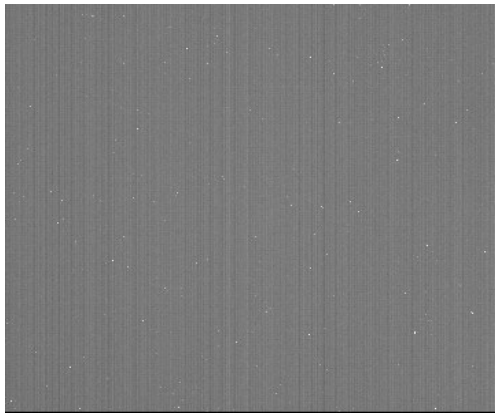


Fig. 5 Load FPGA software system design
图5 载荷FPGA软件系统设计

FU Peng *et al*：High-precision spot centroid positioning of high-frame-rate short-wave infrared images for sat-
ellite laser communication

1 期   71

（a）

（b）

Fig.6　Comparison before and after image correction：(a)original image；(b)post-corrected image

图 6　图像校正前后对比：(a)原始图像；(b)校正后图像

$$\mathrm{NUN} = \frac{1}{\overline{V_s}} \sqrt{\frac{1}{M \times N} \sum_{i=1}^{M} \sum_{j=1}^{N} (V_s(i,j) - \overline{V_s})^2} , \quad (15)$$

where V_s is the response of the pixel (i, j) and $\overline{V_s}$ is the average response gray level of the detector array pixel. The probability density distribution of the ratio of the pixel value to the mean value of the image at each point of the image before and after correction is shown in Fig. 8, and it can be seen that the image response is more dispersed before correction, and the nonuniformity of the image is greatly improved after correction. The non-uniformity of the image before and after correction is reduced from 7% to 0. 6%.

2. 3　Effect of non−uniformity and blind pixels on localization

Figure 9 demonstrates the intensity distribution of the spot before and after correction for non-uniformity when the spot centroid is not at the center of the pixel point. Before correction, the spot is affected by non-uniformity, and the distribution at the edge of the spot is not uniform, and the undulation at the edge of the spot makes the spot size larger and diffuse. After correction, the spot edges are uniformly distributed, and because the
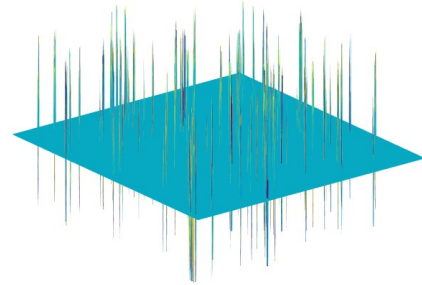

（a）
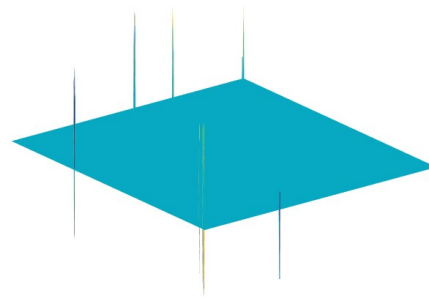
（b）

Fig.7　Comparisons of blind pixels distribution before and after correction：(a)before correction；(b)after correction

图 7　矫正前后盲元分布对比：(a)矫正前；(b)矫正后

spot centroid is not in the center of the pixel, the spot has a certain degree of morphological aberration, which will cause some interference to the accuracy of the centroid positioning.

Figure 10 demonstrates the light spot intensity distribution before and after the non-uniformity correction when the centroid of the light spot coincides with the center of the pixel point. Before correction the spot is affected by non-uniformity, the spot edge distribution is not uniform, the edge appears a certain degree of undulation, after correction the spot edge becomes uniform, at this time the spot on the whole has good symmetry, the light intensity distribution is centrally symmetric, close to the ideal Gaussian distribution of spot morphology, at this time the spot centroid localization accuracy is high.

The ideal spot can be considered to be generated by a Gaussian beam, and its intensity is Gaussian distribution. The electric field intensity of the Gaussian beam in space can be expressed by the complex amplitude and its
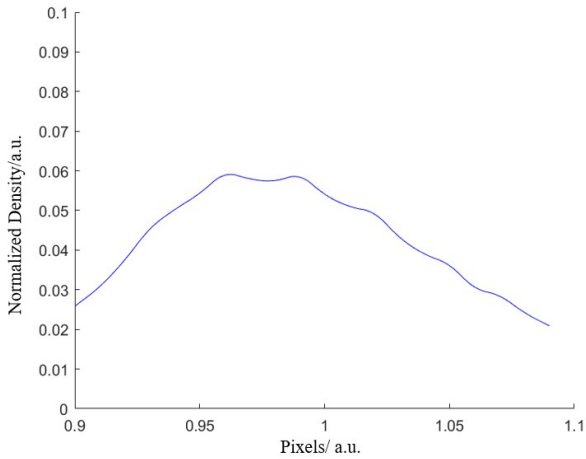
（a）
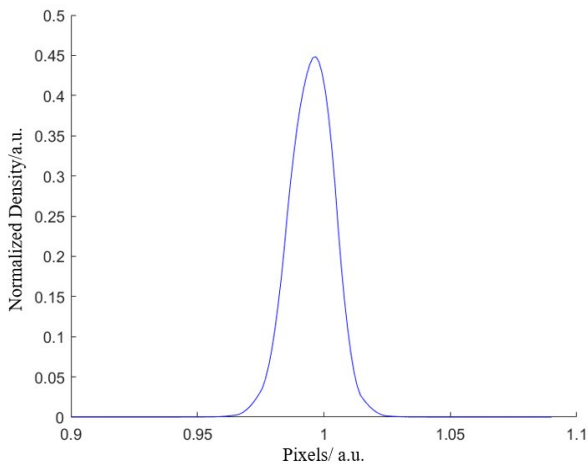
（b）

Fig.8 Comparison of non-uniformity distribution before and after correction：(a)before correction (NUN=0.079 5)；(b)after correction (NUN=0.006 7)
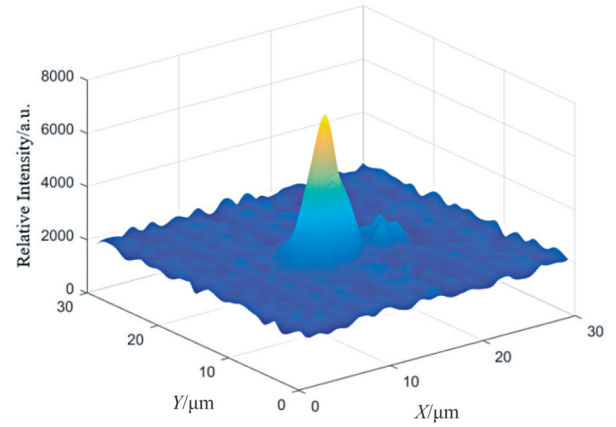图 8 矫正前后非均匀性分布对比：(a)矫正前(NUN=0.079 5)；(b)矫正后(NUN=0.006 7)

（a）

（b）

Fig. 9 Spot intensity distribution before and after correction：(a) original spot；(b)corrected spot
图 9 矫正前后光斑强度分布：(a)原始光斑；(b)矫正后光斑

expression is
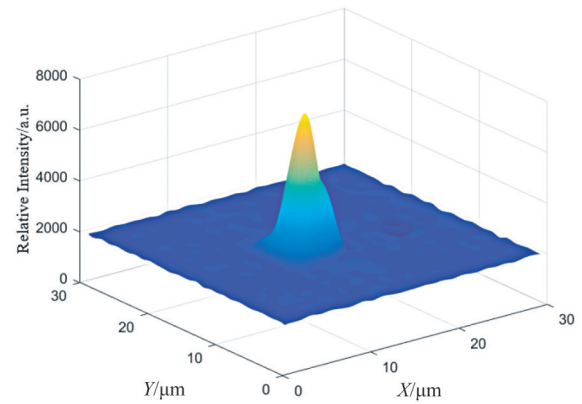
$$E(x,y,z) = \frac{w_0}{w} \exp\left[-\frac{x^2 + y^2}{w^2}\right] \exp\left\{i\left[\frac{x^2 + y^2}{w^2}\right] - \psi\right\} \exp(ikz) \quad , \quad (16)$$

where w_0 is the radius of the center beam waist, $k = \frac{2\pi}{\lambda}$ is the beam, λ is the beam wavelength, w is the beam width at which the beam propagates to z, and ψ is the phase factor.

In short-wave infrared imaging systems, physically damaged detector units as well as detector charge transfer channel obstacles, optical lens defects, etc. will produce blind pixels in the image, and the locations of these blind pixels are fixed. When spot centroid localization is performed, these blind pixels will greatly interfere with the spot localization accuracy.

When the Gaussian surface fitting method is used to locate the centroid of the spot, the maximum point of the spot pixel value and its four adjacent points are used to fit the Gaussian spot to determine the centroid position, and the effect of the blind pixel on the centroid localization is related to the distance of the blind pixel point from the centroid as well as the value of the blind pixel, and the simulation results of the spot localization error are shown in Fig. 11. When the blind pixel point is greater than 2 pixel points from the spot centroid, the blind pixel has no effect on the spot positioning accuracy; when the blind pixel point is 1 pixel point from the spot center, the effect of the blind pixel on the spot positioning error is shown in Fig. 11(a); and when the blind pixel is located at the pixel point in the spot center, the effect of the blind pixel on the spot positioning error is shown in Fig. 11(b). It can be seen that the blind pixel has the greatest influence on the centroid positioning error when it is located at the center point of the spot, and the maximum positioning error can reach up to 1. 3 pixel points, and when the blind pixel is located 1 pixel point away from the center of the spot, the centroid positioning error with the change of the value of the blind pixel stays below 0. 5
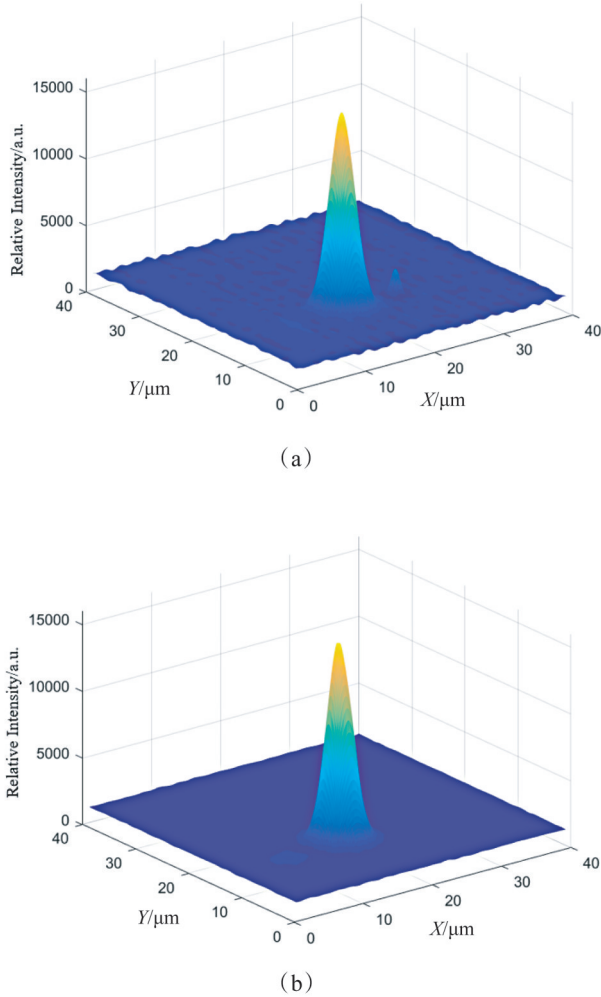
FU Peng *et al*：High-precision spot centroid positioning of high-frame-rate short-wave infrared images for satellite laser communication

1 期

73

（a）

（b）

Fig. 10　Spot comparison before and after correction：(a)original spot；(b)corrected spot
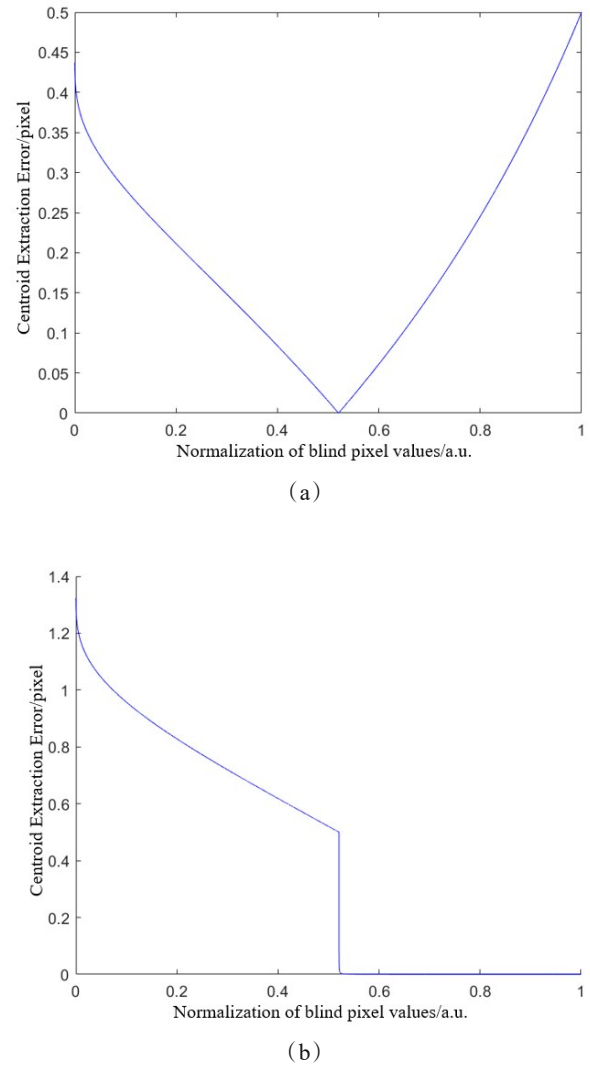
图10　矫正前后光斑对比：(a)原始光斑；(b)矫正后光斑

（a）

（b）

Fig. 11　Influence of the blind pixel on the spot centroid localization accuracy：(a)1 pixel from the center of the spot；(b)the blind pixel is located at the center pixel of the spot

图11　盲元对光斑质心定位精度的影响：(a)距光斑质心一个像素点；(b)盲元位于光斑质心像素点

pixel points.

　　Adopting the blind pixel compensation method of adjacent pixel weighting described herein to process the blind pixels in the spot image，when the blind pixel point is 1 pixel point away from the center of the spot，the blind pixel compensation result is shown in Fig. 12，which can improve the spot centroid positioning accuracy to 0. 0763 pixel points，and when the blind pixel point is located in the center of the spot，the blind pixel compensation result is shown in Fig. 13，which can improve the spot centroid positioning accuracy to 0. 0005 pixel points. The simulation results show that when the blind pixel appears in the spot，the blind pixel compensation method with the weighting of the neighboring pixels can reduce the influence of the blind pixel on the spot positioning accuracy，and significantly improve the spot centroid positioning accuracy.

2. 4　Spot positioning results

　　Using the galvanometer and beacon light to test the positioning accuracy of the load centroid，as shown in Fig. 14. Based on the center of the detector，the spot position is moved by adjusting the deflection radian of the galvanometer X-axis and Y-axis. Fixed galvanometer Y-axis is unchanged，adjust the X-axis galvanometer deflection arc with equal spacing，and then fixed galvanometer X-axis is unchanged，adjust the Y-axis deflection arc with equal spacing，to obtain the spot centroid position of the 13 points shown in the figure. Since the deflection radian of the galvanometer between any two adjacent points is equal，the distance between any two points of the spot centroid position measured theoretically is equal. The centroid positions of these 13 points are measured using loads，and the average value is taken for 50 measurements of a single point. The centroid position spacing before and after the non-uniformity correction is obtained as shown in Fig. 15，the maximum difference between the spacing of two adjacent points obtained before the non-uniformity correction is 0. 5310，which can be considered that the positioning accuracy error is less than 0. 2655 pixel points；the maximum difference between
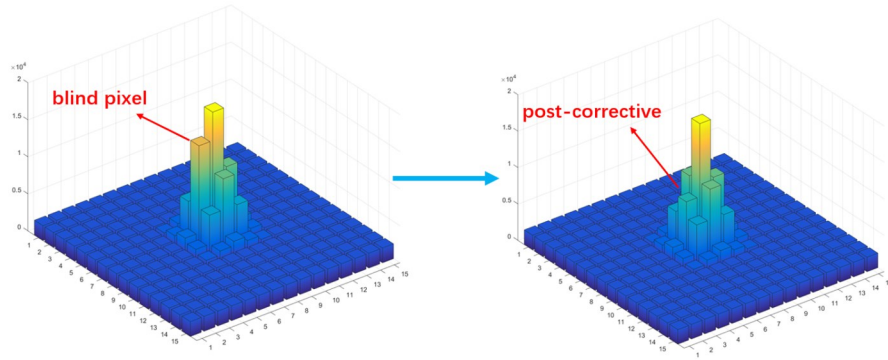
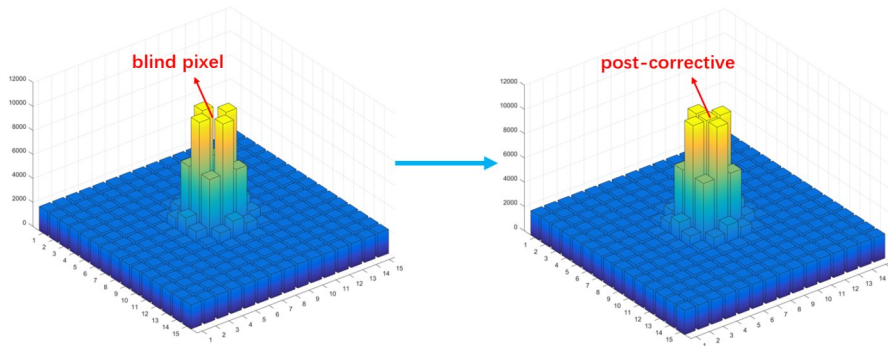Fig. 12　Blind pixel point 1 pixel point from spot center
图12　盲元点距离光斑中心1个像素点

Fig. 13　Blind pixel point at the center of the spot
图13　盲元点位于光斑中心

the spacing of two adjacent points obtained after the non-uniformity correction is 0.1930, which can be considered that the positioning accuracy error is less than 0.0965 pixel points. The localization accuracy after non-uniformity correction is 63.7% higher than that before non-uniformity correction. It can be seen that the distance between adjacent two points remains stable in most cases, and only a few points have large deviations before image correction, resulting in a decrease in positioning accuracy. This is because at this time the spot centroid is close to the middle position of the two pixel points, and the spot centroid localization is prone to large deviations. The short-wave infrared high-precision spot centroid localization method proposed in this paper has a significant increase in the accuracy of the centroid localization when the centroid of the spot deviates from the center of the pixel point, which verifies the correctness of this method.

2.5　Compared with other positioning methods

In order to further verify the effectiveness of the proposed centroid localization method, we choose the energy-weighted localization method in Yang *et al.* [27] as a comparison, and the localization error results are shown in Table 1. Yang *et al.* used median filtering and Gaussian filtering to remove noise and extract laser footprint at the same time. The influence of non-uniformity was eliminated by ellipse fitting method based on least squares, and finally the centroid was obtained by energy weighting. According to Table 1, the centroid positioning error of Gaussian fitting is 0.091 pixels, and the energy-
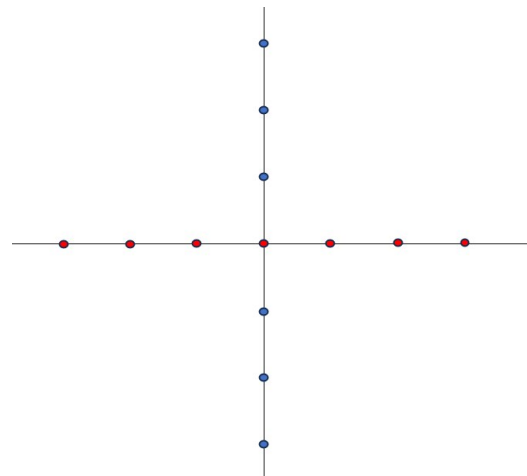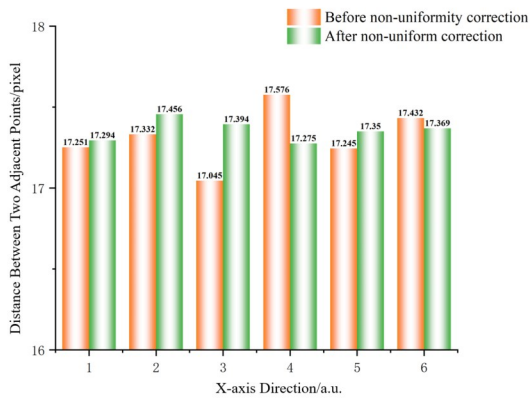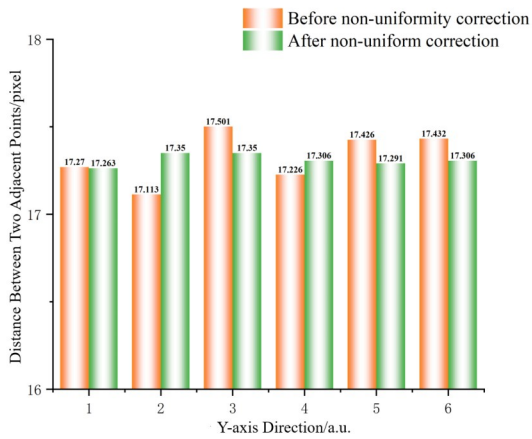

Fig. 14　Spot centroid positioning accuracy test
图14　载荷质心定位精度测试

weighted centroid positioning error is 0.183 pixels, which is greater than 0.1 pixels. The possible reason is that they can not completely eliminate the influence of image non-uniformity by ellipse fitting, while our method has a good effect on this based on the non-uniformity elimination method of calibration. At the same time, they do not make effective processing of blind pixels in the image, and the energy weighting method is more vulnerable to the influence of blind pixels, resulting in insufficient robustness. Therefore, the method proposed in

FU Peng *et al*：High-precision spot centroid positioning of high-frame-rate short-wave infrared images for satellite laser communication

1 期

75

（a）

（b）

Fig.15　Distance between centroid positions before and after image correction：(a)the distance between centroid positions in the *X*-axis direction；(b)the distance between centroid positions in the *Y*-axis direction

图 15　图像矫正前后质心位置间距：(a)*X*轴方向质心位置间距；(b)*Y*轴方向质心位置间距

this paper has better centroid localization performance.

2. 6　Load system design and finished products

Based on the model and simulation，the structure design of the shortwave infrared high-precision spot positioning load designed by us is shown in Fig. 16. The load hardware contains the InGaAs detector，interface board，driver board，control board，and digital transmission communication board，and its structural design is shown in Fig. 16. The interface board provides detector

voltage inputs，the driver board contains DDR，Flash and other memory device drivers，the control board contains FPGAs，and the digital communication board contains Uart and Camlink communication interfaces. The FPGA adopts the XC6LSX75-2FGG484I chip to provide timing drive for the detector and collects the image data output from the detector，as well as processes the collected image data and sends the sought centroid position to the main control through the serial communication module. In addition，through the Camlink interface，the system is able to transmit another way of image data to the host computer.

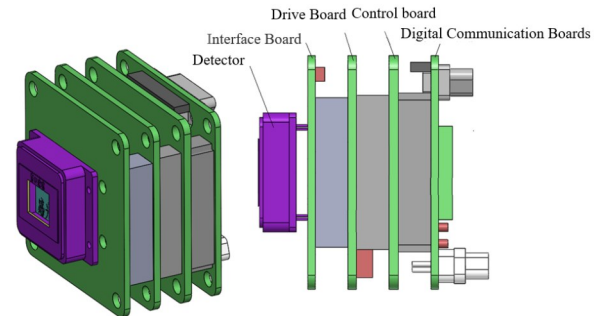
Fig. 16　Schematic diagram of load hardware structure

图 16　载荷硬件结构示意图

The finished product of the load is shown in Fig. 17，which supports high frame rate centroid positioning at 2 000 Hz，with stability and reliability as well as good encapsulation and protection for satellite laser communication.

The load has passed the spaceflight environment screening experiment and loaded on the satellite optical system，achieved good short-wave infrared spot centroid positioning effect，and will be put into use on the satellite at a later stage，as shown in Fig. 18.

3　Conclusions

In this paper，a short-wave infrared high-precision spot centroid localization model is proposed，and the effects of short-wave infrared image non-uniformity and blind pixel on spot centroid localization accuracy are analyzed based on the model. And based on the latest short-wave InGaAs detector and FPGA，a high-frame-frequency short-wave infrared spot centroid localization payload for satellite laser communication was designed for experimental verification. The experimental results show that the non-uniformity of the detector′s original image is reduced from 7% to 0. 6%，the blind pixel compensation rate is close to 100%，and the spot cen-

Table 1　Distance between centroid positions
表 1　质心位置间距

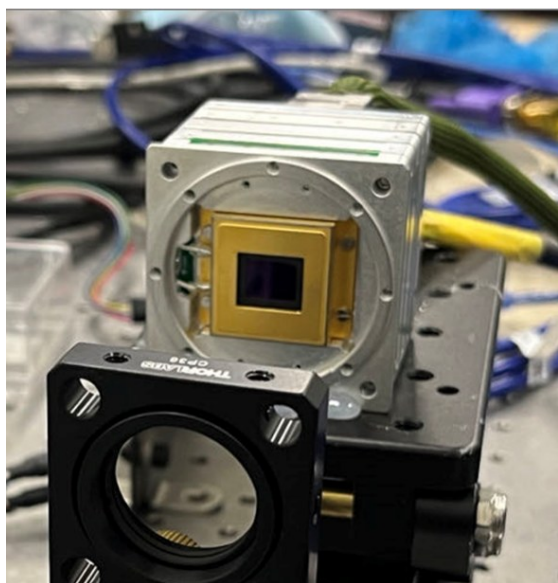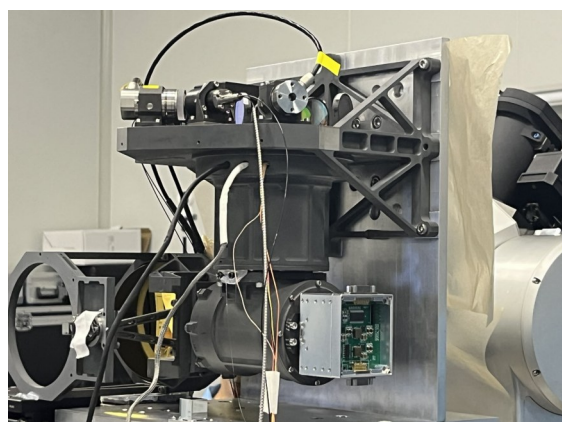| Method	Spacing1 /pixel	Spacing 2 /pixel	Spacing 3 /pixel	Spacing 4 /pixel	Spacing 5 /pixel	Spacing 6 /pixel	Localization error /pixel
Energy weighting method	17. 421	17. 309	17. 173	17. 539	17. 265	17. 465	0. 183
Gaussian fitting method	17. 294	17. 456	17. 394	17. 275	17. 350	17. 369	0. 091

Fig. 17　Finished product
图17　载荷成品

Fig. 18　Satellite opto-mechanical system
图18　卫星光机系统

troid localization accuracy reaches 0. 1 pixel point, the frame rate can be up to 2000 Hz, and the computational delay is less than 500 μs, which can satisfy the demand for high-precision spot centroid localization for the short-wave infrared in satellite laser communication. The short-wave infrared high-precision spot centroid positioning method in this paper is characterized by easy implementation, high real-time performance and strong anti-interference ability, and the payload will be put into use in practical engineering in the future. Due to the constraints of the carrying platform, the laser communication terminal is developing in the direction of lightweight miniaturization, and we will focus on the lightweight miniaturization and low-power consumption of the payload in the future research, which will help to realize the satellite space Internet.

References

［1］GAO Duorui, XIE Zhuang, MA Rong, et al. Development Current Status and Trend Analysis of Satellite Laser Communication［J］. Acta Photonica Sinica（高铎瑞，谢壮，马榕，等. 卫星激光通信发展现状与趋势分析［J］. 光子学报），2021，**50**（04）：0406001.

［2］LIU Xiangnan, LI Chuncai, LI Xiaoliang, et al. New technologies of space laser communication for the space-ground integrated information network［J］. Journal of Telemetry, Tracking and Command（刘向南，李春才，李晓亮，等. 天地一体化信息网络空间激光通信新技术［J］. 遥测遥控），2019，**40**（1）：1-7.

［3］Roberts W T. Discovery deep space optical communications（DSOC）transceiver［C］//Free-Space Laser Communication and Atmospheric Propagation XXIX. SPIE, 2017, **10096**：229-243.

［4］Hanson W A. In their own words：oneweb's internet constellation as described in their FCC form 312 application［J］. New Space, 2016, **4**（3）：153-167.DOI：10.1089/space.2016.0018.

［5］Mcdowell J C. The low earth orbit satellite population and impacts of the spacex starlink constellation［J］. The Astrophysical Journal. Letters, 2020, **892**（2）.

［6］Wilson K E. An overview of the GOLD experiment between the ETS-6 satellite and the table mountain facility［J］. The Telecommunications and Data Acquisition Report, 1996.

［7］Gregory M, Heine F, Kämpfner H, et al. TESAT laser communication terminal performance results on 5.6 Gbit coherent inter satellite and satellite to ground links［C］//International Conference on Space Optics—ICSO 2010. SPIE, 2017, **10565**：324-329.

［8］JIANG Huilin, FU Qiang, ZHAO Yiwu, et al. Development status and trend of space information network and lasercommunication［J］. Chinese Journal on Internet of Things（姜会林，付强，赵义武，等. 空间信息网络与激光通信发展现状及趋势［J］. 物联网学报），2019，**3**（2）：1-8.

［9］Toyoshima M. Recent trends in space laser communications for small satellites and constellations［J］. Journal of Lightwave Technology, 2021, **39**（3）：693-699.

［10］Sodnik Z, Lutz H, Furch B, et al. Optical satellite communications in Europe［C］//Free-space laser communication technologies XXII. SPIE, 2010, **7587**：49-57.

［11］Sodnik Z, Furch B, Lutz H. Free-space laser communication activities in Europe：SILEX and beyond［C］//LEOS 2006-19th Annual Meeting of the IEEE Lasers and Electro-Optics Society. IEEE, 2006：78-79.

［12］Heine F, Mühlnikel G, Zech H, et al. The European Data Relay System, high speed laser based data links［C］//2014 7th Advanced Satellite Multimedia Systems Conference and the 13th Signal Processing for Space Communications Workshop（ASMS/SPSC）. IEEE, 2014：284-286.

［13］Migliore R, Duncan J, Pulcino V, et al. Outlook on EDRS-C［C］//International Conference on Space Optics—ICSO 2016. SPIE, 2017, **10562**：809-817.

［14］Calzolaio D, Curreli F, Duncan J, et al. EDRS-C – The second node of the European Data Relay System is in orbit［J］. Acta Astronautica, 2020, **177**：537-544.

［15］Sun X, Skillman D R, Hoffman E D, et al. Free space laser communication experiments from Earth to the Lunar Reconnaissance Orbiter in lunar orbit［J］. Optics express, 2013, **21**（2）：1865-1871.

［16］DeVoe C E, Pillsbury A D, Khatri F, et al. Optical overview and qualification of the LLCD space terminal［C］//International Conference on Space Optics—ICSO 2014. SPIE, 2017, **10563**：115-123.

［17］Chishiki Y, Yamakawa S, Takano Y, et al. Overview of optical data relay system in JAXA［C］//Free-Space Laser Communication and Atmospheric Propagation XXVIII. SPIE, 2016, **9739**：114-118.

［18］Hanada T, Yamakawa S, Kohata H. Study of optical inter-orbit communication technology for next generation space data-relay satellite［C］//Free-Space Laser Communication Technologies XXIII. SPIE, 2011, **7923**：81-86.

［19］Yamakawa S, Hanada T, Kohata H, et al. JAXA's efforts toward next generation space data-relay satellite using optical inter-orbit communication technology［C］//Free-Space Laser Communication Technologies XXII. SPIE, 2010, **7587**：213-218.

［20］Satoh Y, Miyamoto Y, Takano Y, et al. Current status of Japanese optical data relay system（JDRS）［C］//2017 IEEE International Conference on Space Optical Systems and Applications（ICSOS）. IEEE, 2017：240-242.

［21］JIANG Huilin, AN Yan, ZHANG Yalin, et al. Analysis of the status quo, development trend and key technologies of space laser communication［J］. Journal of Spacecraft TT & C Technology（姜会林，安岩，张雅琳，等. 空间激光通信现状、发展趋势及关键技术分析［J］. 飞行器测控学报），2015，**34**（3）：207-217.

［22］Kim D, Lee S, Kim H, et al. Wide-angle laser structured light sys-

1 期

FU Peng *et al*：High-precision spot centroid positioning of high-frame-rate short-wave infrared images for sat-
ellite laser communication

77

tem calibration with a planar object［C］//ICCAS 2010. IEEE，2010：
1879-1882.

［23］Li Q，Liu L，Ma X，*et al*. Development of multitarget acquisition，
pointing，and tracking system for airborne laser communication［J］.
IEEE Transactions on Industrial Informatics，2018，**15**（3）：1720-
1729.

［24］Zhu Y，Huang Y，Li H，*et al*. Research on APT spot detection algo-
rithm in space optical communication［C］//IOP Conference Series：
Materials Science and Engineering. IOP Publishing，2018，**452**（4）：
042184.

［25］Ren C，Xie J，Zhi X，*et al*. Laser spot center location method for
Chinese spaceborne GF-7 footprint camera［J］. *Sensors*，2020，**20**
（8）：2319.

［26］Singh R，Hattuniemi J M，Mäkynen A J. Analysis of accuracy of la-
ser spot centroid estimation［C］//Advanced Laser Technologies 2007.
SPIE，2008，**7022**：354-359.

［27］Yang X，Xie J，Liu R，*et al*. Centroid extraction of laser spots cap-
tured by infrared detectors combining laser footprint images and de-
tector observation data［J］. *Remote Sensing*，2023，**15**（8）：2129.

［28］Bao J，Xing F，Sun T，*et al*. CMOS imager non-uniformity response
correction-based high-accuracy spot target localization［J］. *Applied
optics*，2019，**58**（16）：4560-4568.

［29］Hardie R C，Baxley F，Brys B，*et al*. Scene-based nonuniformity
correction with reduced ghosting using a gated LMS algorithm［J］. *Op-
tics express*，2009，**17**（17）：14918-14933.

［30］Ratliff B M，Hayat M M，Tyo J S. Radiometrically accurate scene-
based nonuniformity correction for array sensors［J］. *JOSA A*，2003，
20（10）：1890-1899.

［31］Rong S-H，Zhou H-X，Qin H-L，*et al*. Guided filter and adaptive
learning rate based non-uniformity correction algorithm for infrared
focal plane array［J］. *Infrared Physics & Technology*，2016，**76**：
691-697.

［32］Richards A A. Emerging applications for high-performance near-in-
frared imagers［J］. *Thermosense XXIV*，2002，**4710**：450-455.

［33］Ettenberg M H，Lange M J，O'Grady M T，*et al*. Room temperature
640x512 pixel near-infrared InGaAs focal plane array［C］//Infrared
Detectors and Focal Plane Arrays VI. SPIE，2000，**4028**：201-207.

［34］Hoffman A，Sessler T，Rosbeck J，*et al*. Megapixel InGaAs arrays
for low background applications［C］//Infrared Technology and Appli-
cations XXXI. SPIE，2005，**5783**：32-38.

［35］Lange D A，Vu P，Wang S C H，*et al*. 6000-element infrared focal
plane array for reconnaissance applications［C］//Airborne Reconnais-
sance XXIII. SPIE，1999，**3751**：145-158.